Limitations of Gaussian Beam Property Based LDA-Velocity Profile Measurement

Gentaro Yamanaka[1], Stefan Becker[2], Franz Durst[3]

1: Institute of Fluid Mechanics, Universität Erlangen-Nürnberg, Erlangen, gyamanak@lstm.uni-erlangen.de
2: Institute of Fluid Mechanics, Universität Erlangen-Nürnberg, Erlangen, sbecker@lstm.uni-erlangen.de
3: Institute of Fluid Mechanics, Universität Erlangen-Nürnberg, Erlangen, durst@lstm.uni-erlangen.de

Abstract When Gaussian laser beam properties are exploited in laser-Doppler anemometry (LDA), fringe patterns can be produced in the measuring volume of LDA-optical systems that show a linear variation of fringe spacing with position. This effect can be utilized to carry out velocity profile measurements, employing an extended LDA-optical system to yield for every particle passage produces a contribution to the profile data. The theoretical background of LDA-velocity profile measurements is summarised in this paper and experiments are performed to verify the theory.

An extended laser Doppler anemometry (LDA) optical system using a Gaussian laser beam source was designed and built possessing two overlapping fringe systems, one having parallel fringes and the other showing a gradient in the fringe spacing. The first fringe system was employed for conventional LDA-measurements and the second was used to deduce the position of the scattering particles passing the measuring control volume. Velocity measurements with high spatial resolution were supposed to become possible in this way. This is demonstrated for laminar boundary layer velocity profiles. The measurement limitations of the method to deduce from the LDA-measurements instantaneous turbulence properties are outlined.

1 Introduction and Aim of Work

Laser Doppler Anemometry (LDA) (Durst et al. 1976; Albrecht et al. 2003) is a fully developed and nowadays widely used optical velocity measuring technique with some unique features for applications in fluid mechanics. It permits non-intrusive velocity measurements with relatively good time and spatial resolutions and its application does not require velocity calibration. Nevertheless, when LDA-systems are applied for flow velocity measurements, the achievable spatial resolutions are finite due to the finite dimensions of the measuring control volume of conventional LDA-optical systems. The diameter of an LDA-optical system has to be chosen to permit a finite number of fringes to be allocated at a measuring position, yielding the following requirement for local turbulent boundary layer measurements:

$$d_m = N\Delta x \leq \frac{5\delta}{Re_\delta{}^{3/4}} \tag{1}$$

where N is the required number of fringes in the measuring control volume, Δx the fringe spacing, δ the boundary layer thickness and Re_δ the boundary layer Reynolds number. The above formula readily suggests that there is always a highest *Re*-number for the application of every LDA-optical system i.e. in many high *Re*-number flows, LDA-measurements that require corrections to remove the influence of the finite measuring control volume, e.g. see Karlsson and co-workers (1992, 1998) and Durst et al. (1992, 1995). When turbulent boundary layer measurements are carried out at high Re_δ, the requested correction for the finite dimensions of the measuring volume for turbulent quantity become large and these make reliable turbulence property investigations close to walls impossible. Hence, for reliable turbulence property investigations in high Re_δ turbulent flows, LDA-systems are required to possess a higher spatial resolution than that achievable with conventional LDA-optical systems. For this reason, the research and development work of the authors described in this paper was carried

out. It took into account research efforts as described by Strunck et al.(2002, 1994) and Czarske and co-workers (2002). These authors describe in their publications LDA-optical systems with improved spatial resolutions. In order to test the applicability of such systems in turbulent wall bounded flows, the authors performed their own developments in this field for finally carrying turbulent velocity measurements. The outcome of the development work and the velocity measurements is described in this paper.

The first part of the paper summarizes the work that needed to be done to select lasers with good Gaussian beam properties. An Argon-Ion laser and a Nd:YAG-laser were finally chosen and combinedly employed in a LDA-optics yielding two fringe systems in the measuring volume, made up laser beams with 2 different wavelengths. The fringe spacing were measured to prove relationships deduced from the theory for Gaussian beam properties. The Gaussian laser beam theory was employed to yield one fringe pattern with linearly varying fringe spacing. Furhtermore, verification experiments were performed to prove the measured fringe variations agree with the corresponding theoretically described relationships. The proven theory provided afterwards the basis for the final design of the optical system employed to carry out velocity profile measurements in laminar boundary layer flows. The resultant LDA signals were processed to yield velocity profile measurements without traversing the measuring LDA-probe volume.

The last part of the paper considers the measurement properties of the employed LDA-system with respect to turbulent flow property measurements. The sensitivity of the system with respect to noise and the achievable spatial resolution is considered. The position errors due to particle motions parallel to the fringe systems are also considered. From the author's own investigations, the author conclude that LDA-systems, which permit velocity profile measurement by Gaussian beam properties, are not suited to study turbulent flows.

2 Gaussian Beam Properties

Laser beams consist of electromagnetic waves that are coherent, highly monochromatic, consist of a single frequency, are well amplitude-stabilized and show gaussian beam characteristics, see Siegmann (1986). These characteristics of laser light waves are of fundamental importance for the application of lasers in most of the optical measurement methods such as laser Doppler anemometry (LDA).

Laser beams produced by stable laser resonators with finite diameter mirrors can be assumed to possess nearly ideal gaussian beam properties (Siegmann 1986). The mathematical description of the gaussian laser beams can be obtained from text books on lasers (Kogelnik 1965; Kogelnik and Li 1966; Arnaud and Kogelnik 1969; Dickson 1970).

Figure 1 shows the schematic image of a gaussian beam in a specific coordinate system that can be best used to describe the local beam properties. A close look at the theory it becomes clear that the beam waist radius r_w characterizes the propagation of the beam. The normarized electromagnetic field of such a Gaussian beam can be mathematically expressed as:

$$E(x,y,z) = \left(\frac{2}{\pi}\right)^{1/2} \frac{1}{r(z)} \exp\left[-\frac{x^2+y^2}{r(z)^2}\right] \exp\left[-jkz + j\phi(z) - jk\frac{x^2+y^2}{2R(z)}\right], \tag{2}$$

where (x, y, z) are the coordinates with their origins at the center of the waist of the Gaussian beam, k is the wave number and $r(z)$ the local radius of beam, defined by the width at the location where the light intensity falls to $1/e^2$ compared to the maximum value in the plane z = const.

The quantity $\phi(z)$, used in eq. (2), is called the Guoy phase shift (Siegmann 1986) and can be formulated as:

$$\phi(z) = \arctan\frac{z}{l_R}. \tag{3}$$

where l_R is called the Rayleigh length and is defined as:

$$l_R = \frac{\pi r_w^2}{\lambda}. \tag{4}$$

Equation (3) can be used to compute the Guoy phase shift and it turns out to be small when the position is near to the waist of a laser beam. Hence, the term in equation (2), giving the Guoy phase shift, can be neglected in the analysis of the fringe system generated at the crossing point of two beams that overlap each other at their waists.

There are other important parameters of the Gaussian laser beam that can be also related to the waist radius r_w and the Rayleigh length l_R, introduced into beam considerations, according to the following equations:

$$r(z) = r_w \sqrt{1 + \left(\frac{z}{l_R}\right)^2}, \qquad \text{(Local beam radius)} \tag{5}$$

$$R(z) = z\left\{1 + \left(\frac{l_R}{z}\right)^2\right\} = z + \frac{{l_R}^2}{z}. \qquad \text{(Local curvature of wavefront)} \tag{6}$$

When a Gaussian beam passes through a lens, the beam is focused in a particular and very characteristic manner. Due to its Gaussian beam properties, the waist locations are given in a particlar manner and Fig. 2 shows some special features of such a focused beam. The waist location after the focussing lens does, in general, not occur at the focal point of the lens, if $z_a \neq F$ as shown in Fig. 2. Its position and radius are depended on the focal length of the lens and the location z_a of the waist before the lens:

$$z_b = F + \frac{(z_a - F)F^2}{(z_a - F)^2 + {l_{R_a}}^2}, \tag{7}$$

$$r_{w_b} = \frac{r_{w_a} F}{\{(z_a - F)^2 + {l_{R_a}}^2\}^{1/2}}, \tag{8}$$

where l_{R_a} is the Rayleigh length at the waist position before the lens.

The equations (7) and (8) shown above explain well the properties of focussed gas laser beams or solid-state ones. Using the Gaussian beams, the design of an LDA-optics with special properties of the fringe systems became easy, and all the theoretical relationships for the properties of Gaussian beams could be easily compared with experiments. In all their experiments the authors employed a frequency-doubled diode pumped solid-state (DPSS) Nd:YAG laser and an Argon-Ion laser for their investigations, both showing good Gaussian beam properties.

3 Theoretical Investigations and Experimental Verifications

3.1 Fringe System Properties and Performance of Extended LDA-Systems

Figure 3 shows the schematic diagram of a typical LDA sending optics with beam expansion. It also indicates parameters like focal lengths of the three lenses used in such a LDA optics and distances between lenses and waists to describe fringe spacings in the overlapping region of two laser beams in the sec. 3.2. It is common practice to cross laser beams, with a finite angle between them, to yield the basic beam arrangement from LDA-velocity measurements. This situation is sketched in Fig. **??** and Fig. 4 indicating two Gaussian light beams that overlap in a typical manner for LDA-optical systems. If such systems are not set up with care, the center point of both beams in the overlap region, i.e. the origins of the *x*-*y*-*z*-coordinate systems, are not identical to two different waist points of the

two beams. Because of this, the fringe spacing is not constant for this considered general case of two overlapping Gaussian laser beams. For the beams arrangement in Fig. 4, diverging fringes are resulted and this has been shown by Hanson (1973) and Durst & Stevenson (1976). A complete analysis was provided by Miles (1996) who showed that the fringe spacing Δx can be expressed as follows,

$$\Delta x = \frac{\lambda}{2\sin\alpha}\left(1 + \frac{z\cos^2\alpha(z\cos^2\alpha - z_w)}{{l_R}^2\cos^2\alpha - z_w(z\cos^2\alpha - z_w)}\right). \tag{9}$$

Especially at $x = z = 0$,

$$\frac{1}{\Delta x}\frac{d\Delta x}{dz} = -\frac{z_w}{{l_R}^2 + (z_w/\cos\alpha)^2} = \frac{\cos\alpha}{R(z_t)} \tag{10}$$

could be obtained. With some approximation, eq. (10) is given by

$$\frac{1}{\Delta x}\frac{d\Delta x}{dz} = -\frac{(z_4 - F_3)\cos^2\alpha}{{F_3}^2}, \tag{11}$$

where z_4 defines the distance from a transmitting lens to the waist position before the lens and F_3 is the focal length of the transmitting lens.

To verify the applicability of the Gaussian beam theory, the fringe spacing distributions by two spritted He-Ne laser beams with changing the distance of the two lenses of a collimator was measured with the same experimental apparatus. by Durst & Stevenson (1979). Figure 8 compared the measured results, indicated with circle plots, with the theoretical values shown in solid lines. From the figure, the experimental results agreed well with the theoretical ones, and it was confirmed that the theory express the realistic properties of the fringe systems interfered by two Gaussian beams. But, there were reveal discrepancies between experiment and theory in the outer region of the measurement volume. These discrepancies came from aberrations of sphere optical lenses.

As described above, the gradient of a fringe spacing distribution can be detected by changing the waist positions of two transmitting beams. Hence, if there are two measurement volumes at the same position and each measurement volume has a different divergence, the position of the path of a particle can be obtained from the following relationship:

$$U(z) = f_{D_A} \cdot \Delta x_A(z) = f_{D_B} \cdot \Delta x_B(z), \tag{12}$$

where f_{D_A} is the Doppler frequency obtained from the signal by one of the two measurement volumes, f_{D_B} is that from the other, and $\Delta x_A(z)$ and $\Delta x_B(z)$ are the fringe spacings in the two measurement volumes at the position z respectively. To achieve this condition, a special LDA-system was employed and this is sketched in Fig. 5.

In the system shown in Fig. 5, the waist positions of the first of two LDA-systems were carefully located with respect to each other to yield a system of parallel fringes all having the same fringe spacing. The second measuring volume of the optical system in Fig. 5 was arranged in such a way that the two beams, which were produced from a Nd:YAG laser, resulted in linearly diverging fringes. The two Nd:YAG beams were arranged in such a manner, that they resulted in a measuring volume located perpendicular to the measuring volume of the Argon-Ion LDA optics. This is sketched in Fig. 6. Hence, the complete optical measuring volume consisted of two overlapping volumes made up of laser beams of different colors;

1. One possesed parallel interference fringes of equal distance Δx permitting the detection of LDA-signals for particle velocity measurements in a conventional way.

2. The second volume located perpendicularly showed linearly diverging fringes yielding an additional LDA-signal for particle position measurements.

As shown in the Fig. 6, only a part of the measurement volumes overlap each other. At a particular position in the *z*-direction, the fringe spacing in the each volume could be expressed as

$$\Delta x_A = \frac{\lambda_A}{2\sin\alpha_A} \tag{13}$$

$$\Delta x_B(z) = \Delta x_B + \left(\frac{d\Delta x_B}{dz}\right)_{z=0} z + \frac{1}{2}\left(\frac{d^2\Delta x_B}{dz^2}\right)_{z=0} z^2, \tag{14}$$

where the subscript of *A* means fringe spacing in the measuring volume of the Argon-Ion LDA-system, i.e. the parallel fringe system, and *B* is the fringe spacing for the Nd:YAG system of diverging fringes. If a particle passes the overlapping region of those two measurement volumes, the velocity of the particle $U(z)$ of *x* component can be written as

$$U(z) = f_{D_A}\Delta x_A \tag{15}$$

where f_{D_A} is a Doppler shift frequency detected by the parallel fringe system. The velocity $U(z)$ is as same for the system with diverging fringes as follows:

$$U(z) = f_{D_A}\Delta x_A = f_{D_B}\left(\Delta x_B + \frac{d\Delta x_B}{dz} z + \frac{1}{2}\frac{d^2\Delta x_B}{dz^2} z^2\right). \tag{16}$$

Hence, taking the difference between eqs. (15) and (16), the following equation can be obtained:

$$\frac{f_{D_A}\Delta x_A - f_{D_B}\Delta x_B}{f_{D_B}} = \frac{d\Delta x_B}{dz} z + \frac{1}{2}\frac{d^2\Delta x_B}{dz^2} z^2. \tag{17}$$

If the fringe spacing is regarded as linear, the second term of the right side hand in eq. (17) can be neglected and the position information *z* can be expressed as

$$z = \left(\frac{f_{D_A}}{f_{D_B}}\Delta x_A - \Delta x_B\right)\left(\frac{d\Delta x_B}{dz}\right)^{-1}. \tag{18}$$

3.2 Design of Optical Arrangements for LDA-Systems with Two Different Fringe Systems

The two fringe systems used for the extended LDA-system are designed based on the LDA-system described in Fig. 3, because the LDA-system is typical and flexible for optical arrangements. The LDA-system consisted of a laser source, a collimator with two lenses of F_1 and F_2, a beam splitter without an optical path difference and a transmitting lens with a focal length of F_3. The z_1, z_2, z_3, z_4 and z_5 are distances between a waist of the laser beam and a lens, as shown in Fig. 3.

To express every information as a function of z_2, we set the three lenses in accordance with the relationships given below;

$$z_0 = z_1 = F_1 \tag{19}$$

$$z_2 + z_3 + z_4 = 2F_2 + F_3. \tag{20}$$

From eqs. (8) and (19), the radius of the waist after the lens1 is given by

$$r_{w_1} = \frac{r_{w_0} F_1}{l_{R_0}}. \tag{21}$$

Hence, a radius and a position of the waist after a collimator become

$$r_{w_2} = \frac{r_{w_1} F_2}{\sqrt{(z_2 - F_2)^2 + {l_{R_1}}^2}} \tag{22}$$

and

$$z_3 = F_2 + \frac{{F_2}^2(z_2 - F_2)}{(z_2 - F_2)^2 + {l_{R_1}}^2}. \tag{23}$$

A radius and a positions at the waist after a transmitting lens are expressed as

$$r_{w_3} = \frac{r_{w_2} F_3}{\sqrt{(z_4 - F_3)^2 + {l_{R_2}}^2}} \tag{24}$$

and

$$z_5 = F_3 + \frac{{F_3}^2(z_4 - F_3)}{(z_4 - F_3)^2 + {l_{R_2}}^2}. \tag{25}$$

However, by substituting eqs. (20), (23) into eqs. (24), (25), the position and the radius could be shown as functions of z_2. For the extended LDA, the gradient of fringe spacings and the length of a measurement volume are very important, because they are related to uncertainty to detect a position of a particle in a measurement volume and a measurable range. The gradient of fringe spacings can be obtained as

$$-\frac{1}{\Delta x}\frac{d\Delta x}{dz} = \frac{(z_5 - F_3)}{(l_{R_3}\cos\alpha)^2 + (z_5 - F_3)^2}\cos^2\alpha. \tag{26}$$

by substituting $z_w = z_5 - F_3$ into eq. (10), and the length of a measurement volume becomes

$$l_{MV} = 2r_{w_3}\sqrt{1 + \left(\frac{z_5 - F_3}{l_{R_3}}\right)^2} / \sin\alpha. \tag{27}$$

Actually, the diverging LDA-system employed the arrangement shown in Fig. 7 to make its size be small. But, there is no difference from the arrangement shown in Fig. 3 except the shape of a beam splitter. From these calculation, the parameters are decided and predicted as shown below:

F_1 : 16 mm,
F_2 : 100 mm,
F_3 : 300 mm,
z_2 : 101.24 mm.

On the other hand, the concept of the design for the parallel fringe system is that the change of the fringe spacing by the Argon-Ion laser should be as small as possible in the overlapping region. To accomplish the requirement, the diameter of the measurement volume for the system should be relative large by the following reasons. The eq. (9) shows the distribution of fringe spacings. When the two laser beams separated by a beam splitter intersect at each waist position, the equation can be rewritten as

$$\Delta x = \frac{\lambda}{2\sin\alpha}\left(1 + \frac{z^2}{{l_{R_3}}^2}\cos^2\alpha\right). \tag{28}$$

Because l_{R_3} in the above equation is constant, it reveals that the fringe spacing distribution can be assumed as parabolic. To reduce the effect of the parabolic distribution, the diameter of each beam should be large, because l_{R_3} can be expressed as eq. (4). Threrefore, the specification of the optics was decided;

F_1 : 20 mm,
F_2 : 50 mm,
F_3 : 363 mm.

4 Laminar Velocity Profile Measurements

4.1 Experimental Apparatus

The experimental apparatus consists of the extended LDA-system, a wind tunnel to generate a flow and a glass plate to make a wall boundary layer.

Since the extended LDA-system are detailedly described in the sec. 3, the spacifications of optical devices and data processing devices are explained here. The Argon-Ion laser source is manufactured by Ion Laser Technology (Utah, USA), its laser power is changeable up to 140 mW. In all experiments, we set the laser power at 80 mW. The size of the measurement volume for the Argon-Ion LDA-system is defined by the length of 3977 μm, the diameter of 275.5 μm and the depth of 275.5 μm. The distribution of the fringe spacing is shown in Fig. 9.

On the other hand, the Nd:YAG laser source is manufactured by Coherent, Inc. (Santa Clara, USA), and its laser power is 100 mW. The size of the measurement volume is defined by the length of 2616 μm, the diameter of 130.8 μm and the depth of 130.7 μm. The distribution of the fringe spacing is shown in Fig. 10.

For each LDA-system, an avalanche photodiode (APD) was located in the forward direction. A lens was located before each APD, on which scattered light from particles was forcused. Each APD is connected to a TSI-1980 counter (TSI, USA) to detect Doppler frequencies from scattered light. The two counters were connected to a PC to acqire velocity informations. From the two kinds of acquired velocity informations, i.e. from the Argon-Ion system and the Nd:YAG system, positions of particles were obtained.

The wind tunnel is a Göttingen type and the wind velocity at the outlet is from 0 to 9 m/s. To generate a wall boudary layer flow, a glass plate is set at the outlet of the wind tunnel.

4.2 Velocity Profile Measurement

Figure 11, on which the series of instantanious velocity data were ploted, shows the raw velocity profile in a laminar boundary layer at $x = 185$ mm downstream from the edge of a plate. In the figure, the vertical axis is the normalized velocity by U_∞, where U_∞ is the velocity far from the wall. the holizontal axis stands for non-dimensional position $\eta = \frac{z}{x} {Re_x}^{1/2}$, where Re_x is the Reynolds number based on the position x and the velocity U_∞. In Fig. 11, the yellow plots were the averaged velocities obtained by a conventional LDA-system. By the comparison between the data by the extended LDA and that by the conventional one, both results agreed well. However, the reliability of the extended LDA-system could not be discussed here, because the knowledge from Fig. 11 is only that the measured instantanious velocities by the extended system converge to the data by the conventional method.

Figure 12 shows the averaged velocity profile calcurated from the same data shown in Fig. 11. The figure shows that the gradient of measured velocities does not agree with the Blasius's profile. This is caused by the uncertainty of the position detection by the extended LDA.

The uncertainty δz of the position z measured with the extended LDA-system can be defined as

$$\delta z = \left[\left(\frac{\partial z}{\partial f_{D_A}} \right)^2 \delta {f_{D_A}}^2 + \left(\frac{\partial z}{\partial f_{D_B}} \right)^2 \delta {f_{D_B}}^2 + \left(\frac{\partial z}{\partial \Delta x_A} \right)^2 \delta {\Delta x_A}^2 + \left(\frac{\partial z}{\partial \Delta x_B} \right)^2 \delta {\Delta x_B}^2 + \left(\frac{\partial z}{\partial A} \right)^2 \delta A^2 \right]^{1/2}, \quad (29)$$

where A is $\partial \Delta x_B / \partial z$. By substituting certain values into the eq. (29), the uncertaininy of the position detection by the extended LDA could be estimated as 162 μm. In the left hand side of the eq. (29), the effects of the 3rd and 4th terms on the size of the uncertainty were dominant. The 3rd and 4th terms are caused by the uncertainities of two fringe spacings, and directly depends on the stability of the motor used in calibrations. In the research, the uncertainities of a parallel fringe system $\delta \Delta x_A$ and a

gradient one are $\delta\Delta x_B$ are 1.52×10^{-2} μm and 2.02×10^{-2} μm respectively. A stabilized motor should be used for caliblations to reduce these two terms. However, their values become the one-tenth of the present values at the best. In such a case, the estimated uncertainty for the position detection is considered as 10 μm order.

The uncertainty is the same meaning as a spatial resolution of the extended LDA-system, and affects statistical values of measured velocities, i.e. averaged velocity and standard deviation. The following explains the effect of the spatial resolution on an averaged velocity.

In Fig. 13, the solid line is an averaged velocity profile, the dushed is the maximum limit of instantanious velocities, and the dush-dot is the minimum ones. In the measurement by the conventional method, measured instantanious velocities occupy at a certain area with the width of the measurement volume diameter d_m. The area is colored in blue in Fig. 13. In the measurement by the extended LDA, however, the method detects a position of a particle and has a spatial resolution δz, and it is considered that the left side border of the area and the right one are shifted with a length of the spatial resolution δz to the left and the right respectively.

The shift of the border of an actual instantanious velocity area means that the actual velocity fields are stretched into the abscissa, and effects a averaged velcity at a position. The mechanism of the effect on the averaged velocity is imaged in Fig. 13. The red solid line in the figure stands for an averaged velocity profile measured by the extended LDA. It shows that the measured averaged velcity profile fits with the acutual velocity profile in only the region whose width is "$d_m - 2\delta z$". This is the reason that the gradient of the averaged velocity profile, in a laminar boundary layer measured by the extended LDA, does not fit to the Blasius's velocity profile in Fig. 12.

5 Measurement of Turbulence Properties

Experiments are performed at the same apparatus as the laminar flow experiments. To induce sudden turbulent transition, the sandpaper was set at the entrance of the plate.

Figure 14 shows the averaged velocity profiles. The spurious data are removed with the post-data-processing which is explained in the section 4.2. Since the number of data samples at a position is not enough, the averaged velocities are scattered. However, the velocities converge to a certain value at a position, if the experiments are repeated and the number of samples is enough. It could not recognize that the gradient of averaged velocities agree with the acutual one. But it is considered that the gradient of the averaged velcity profile does not fit to the acutual velocity profile because of the reason which was discribed in the section 4.2.

On the other hand, Fig. 15 shows the distribution of standard deviation compared with that measured by the conventional method. The standard deviations by the extended LDA seems larger than that by the conventional method in a buffer region. It is considered that the fluctuation of the position detection by the extended LDA-system induces extra velocity fluctuations. This is explained in details as follows.

The velocity fluctuation measured by the conventional method is analyzed by Durst et al. (Durst et al. 1992) and is expressed as

$$v_{meas}^2 = v_{true}^2 + \frac{{d_m}^2}{16}\left(\frac{\partial \overline{U}}{\partial y}\right)^2 \tag{30}$$

where the subscript *meas* means the measured value, that of "*true*" is the true value, and d_m is the diameter of a measurement volume.

In the case for the extended LDA, the error of the turbulent intensity caused by the size of a spatial resolution also exists and eq (30) can be rewritten as

$$v_{meas}^2 = v_{true}^2 + \frac{\delta y^2}{16}\left(\frac{\partial \overline{U}}{\partial y}\right)^2 \tag{31}$$

using the spatial resolution "δy". In the experiment, the spatial resolution "δy" is 160 μm and the error of the turbulent intensity caused by the spatial resolution size become bigger than that of a conventional method. Futhermore, there is a error caused by the uncertainity of a position detection, which comes from eq. (18). Therefore, the error of the turbulent intensity caused by the summention of these two uncertainities and becomes bigger than the actual value.

Finally, it should be menthined that the error of the turbulent intensity also comes from other reasons, i.e. shot noise of a photo detector, the particles not passing normal to measurement volumes, etc. But It is difficult to separate the effect of each cause from the others.

6 Conclusions, Final Remarks and Outlook

The extended LDA-system is developed to make precise velocity measurement in the vicinity of a wall, and the following knowledge has been proposed.

1. The uncertainty of velocity detection directly affects that of position detection, i.e. spatial resolution. Therefore, the uncertainty of fringe spacings is the largest factor for the spatial resolution of the extended LDA.

2. The spatial resolution of the extended LDA is estimated as 162 μm from the uncertainty analysis. Compared with conventional LDA, It is not improved. It can be improved by using a speed-stabilized motor, because a motor speed stability used in caliblations directly affect the prediction of fringe spacings. However, if such a stabilized moter is used in caliblations, the uncertainty of the fringe spacings becomes the one-tenth of the present research at the most. Therefore, the uncertainty of a system similar to the extended LDA might be 10 μm order at the best.

3. The spatial resolution affects the gradient of an measured averaged velocity profile in the region except the center of the measurement volume width of "$d_m - 2\delta$". Therefore, if the relatively long measurement volume compared to the spatial resolution could be made, the region which agrees with the actual velocity gradient is large.

4. By the effect of the spatial resolution, the measured turbulent intensity becomes larger than that of a conventional method. This knowledge indicates the system similar to the extended LDA, i.e. the method which detects the positon of a particle in a measurement volume with the gradient of fringe systems, should be carefully applied to turbulent flow measurements.

References

Albrecht HE; Borys M; Damaschke N; Tropea C (2003). *Laser Doppler and phase Doppler measurement techniques*. Springer.

Arnaud JA; Kogelnik H (1969). Gaussian light beams with general astigmatism. *Applied Optics* 8: 1687–1693.

Czarske J; Büttner L; Razik T; Müller H; Dopheide D (2002). Spatial–resolved velocity measurements of shear flows with a novel differential doppler velocity profile sensor. In *Proc. 11th Int Symp on Appl. of Laser Tech. to Fluid Mech.*, 21.1, Lisbon.

Dickson LD (1970). Characteristics of a propagating gaussian beam. *Applied Optics* 9: 1854–1861.

Durst F; Jovanovic J; Sender J (1995). LDV measurements in the near-wall region of a turbulent pipe flow. *J. Fluid Mech.* 295: 305–335.

Durst F; Melling A; Whitelaw J (1976). *Principles and practice of laser–Doppler anemometry*. London: Academic Press.

Durst F; Mrtinuzzi R; Sender J; Thevenin D (1992). LDA–measurement of mean velocity, rms-values and higher order moments of turbulence intensity fluctuations in flow fields with strong velocity gradient. In *6th Int. Sympo. Appl. Laser Tech. Fluid Mech.*, S5–1, Lisbon.

Durst F; Stevenson WH (1976). Visual modeling of laser Doppler anemometer signals by moiré fringes. *Applied Optics* 15: 137–144.

Durst F; Stevenson WH (1979). Influence of gaussian beam properties on laser Doppler signal. *Applied Optics* 18: 516–524.

Hanson S (1973). Broadening of the measured frequency spectrum in a diffrential laser anemometer due to interference plane gradient. *J. Phys. D* 6: 164–171.

Karlsson R; Eriksson J; Persson J (1992). LDA measurement in a plane wall jet in a large enclosure. In *6th Int. Sympo. Appl. Laser Tech. Fluid Mech.*, Lisbon, pp. 1.5.1–1.5.6.

Karlsson R; Johansson T (1998). LDV measurement of higher order moments of velocity fluctuations in a turbulent boundary layer. In *Laser Anemometry in Fluid Mechanics-III*, pp. 273–289. Lisbon: LADOAN.

Kogelnik H (1965). Imaging of optical mode – resonators with internal lenses. *Bell Syst. Tech. J.* 44: 455–494.

Kogelnik H; Li T (1966). Laser beams and resonators. *Applied Optics* 5: 1550–1567.

Miles PC; Witze PO (1996). Evaluation of the gaussian beam model for prediction of LDV fringe fields. In *Proc. 8th Int Symp on Appl. of Laser Tech. to Fluid Mech.*, 40, Lisbon, pp. 11–17.

Siegmann AE (1986). *Laser*. Mill Valley: University Science Books.

Strunck V; Kisters T; Dopheide D (2002). Spatial–resolved velocity measurements of shear flows with a novel differential doppler velocity profile sensor. In *Proc. 11th Int Symp on Appl. of Laser Tech. to Fluid Mech.*, 21.1, Lisbon.

Strunck V; Sodomann T; Müller H; Dopheide D (1994). Fringe field quantification in an LDV probe volume by use of a magnified image. *Exp Fluids* 16: 330–335.

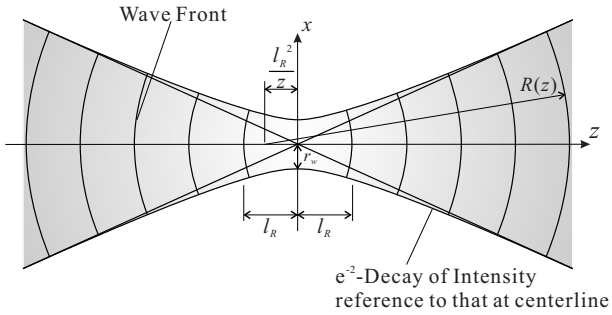

Figure 1: Gaussian Laser beam and Wave Coordinate System

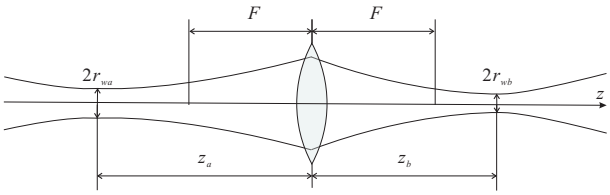

Figure 2: Gaussian Laser Beam Imaged by a Lens

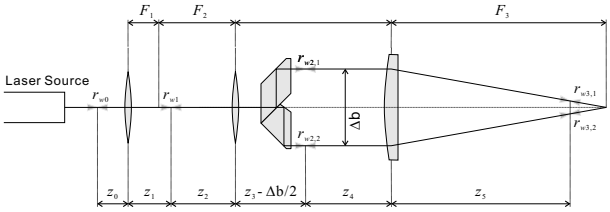

Figure 3: Schematic Diagram of a Typical LDA Optics with beam expansion

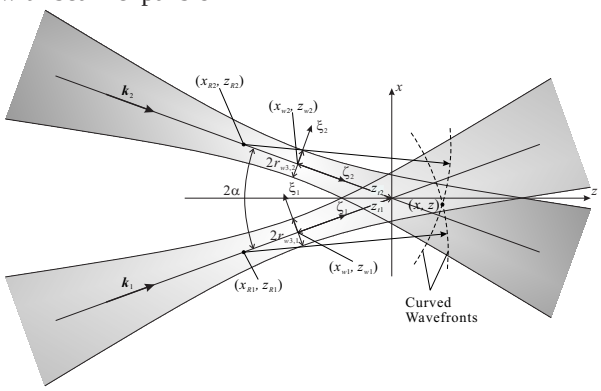

Figure 4: Geometry and Coordinates for Deriving Fringe Spacing

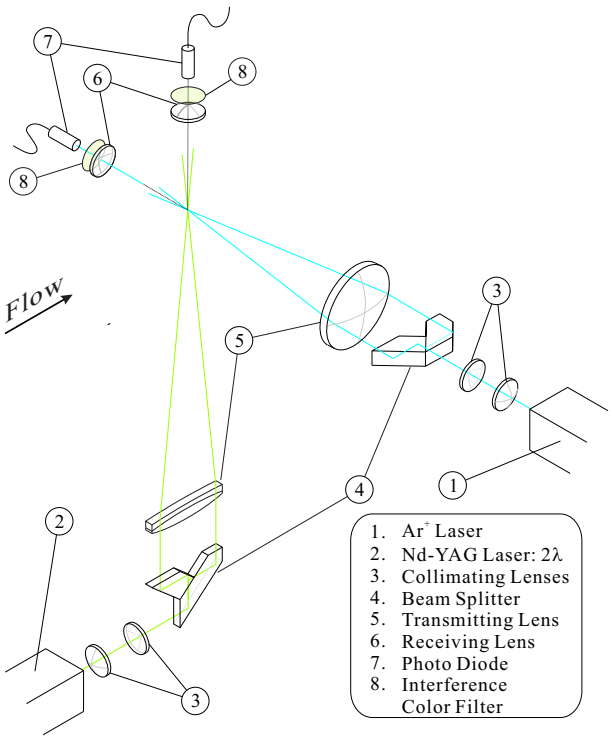

Figure 5: Schematic Diagram of an Extended LDA-System

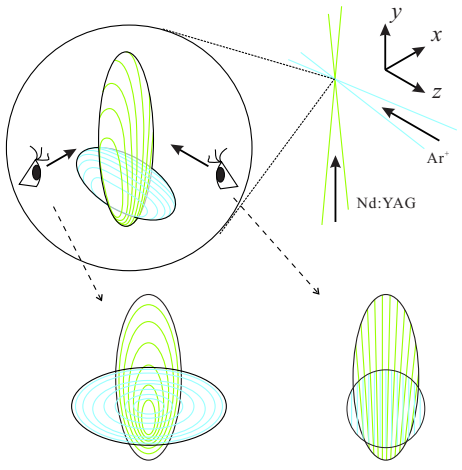

Figure 6: Layout of Two Measurement Volumes

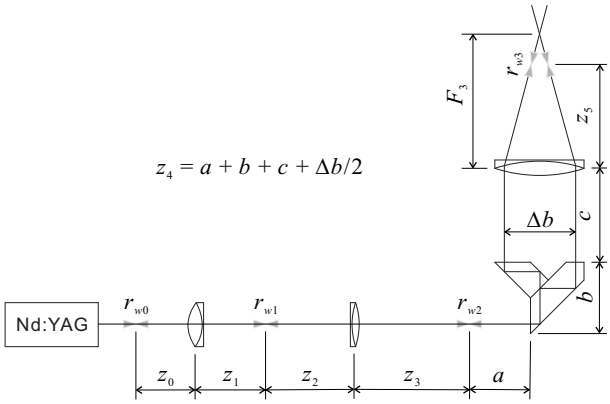

Figure 7: Schematic Diagram of Optics

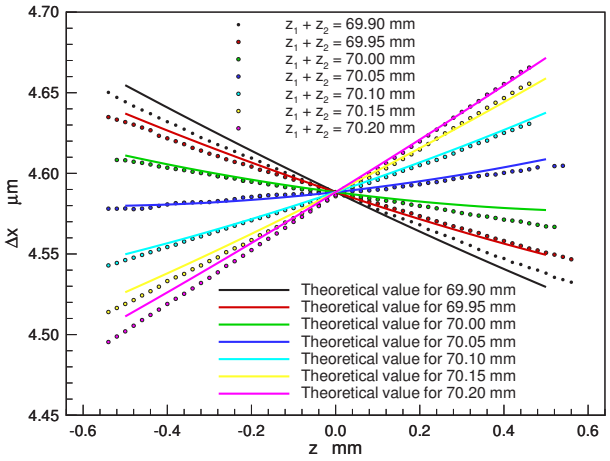

Figure 8: Fringe Spacing Distributions along the Center Line of the Measurement Volume

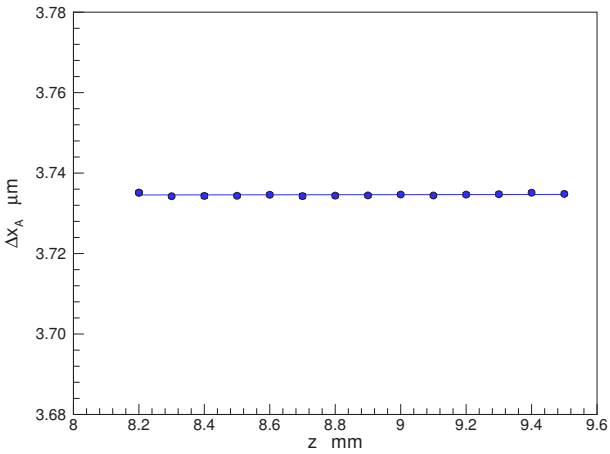

Figure 9: Distribution of the Parallel Fringe System

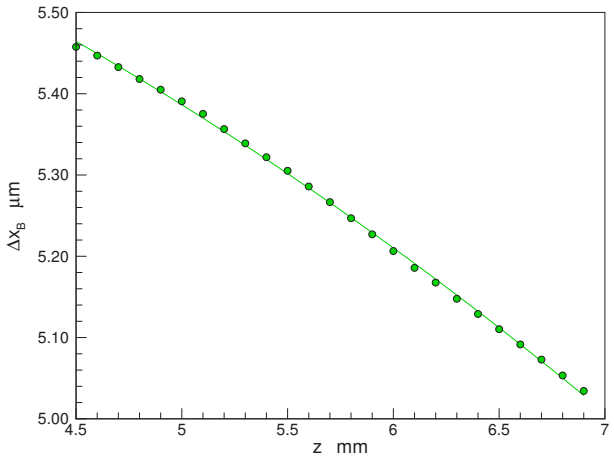

Figure 10: Distribution of the Gradient Fringe System

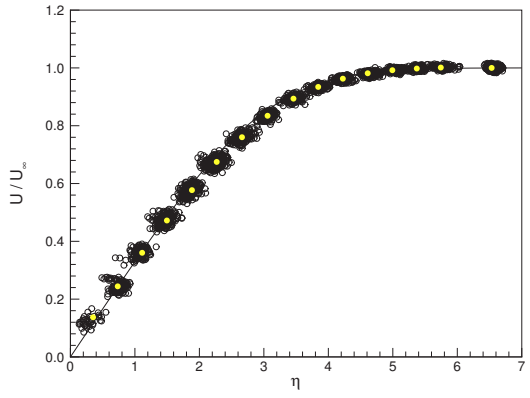

Figure 11: Measured Velocity Profile of the Laminar Boundary Layer (x = 185 mm, U_∞ = 8.5 m/s)

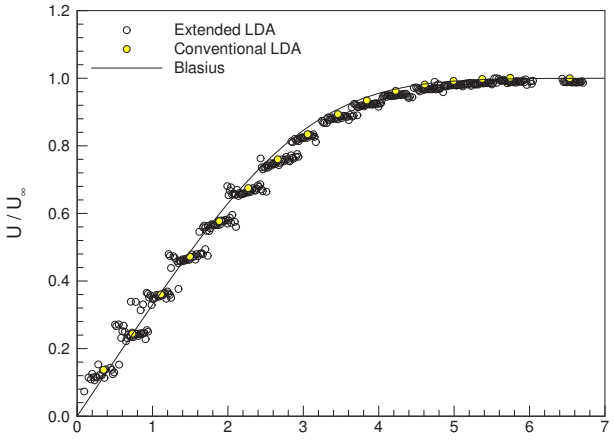

Figure 12: Averaged Velocity Profile of the Laminar Boundary Layer at x = 185 mm

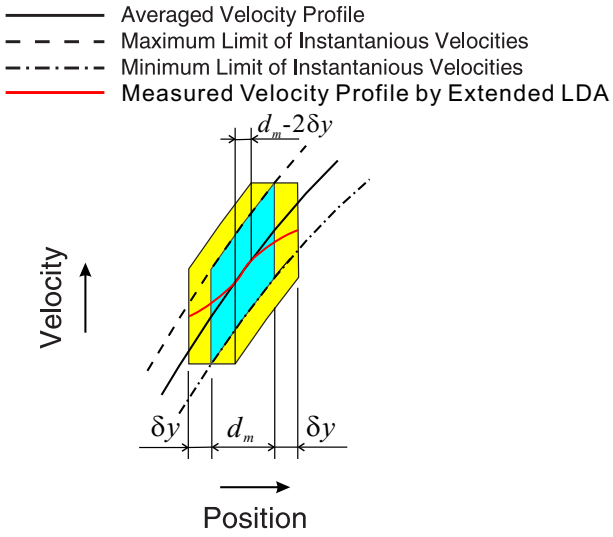

Figure 13: Image of the Stretch of a Velocity Distributed Area

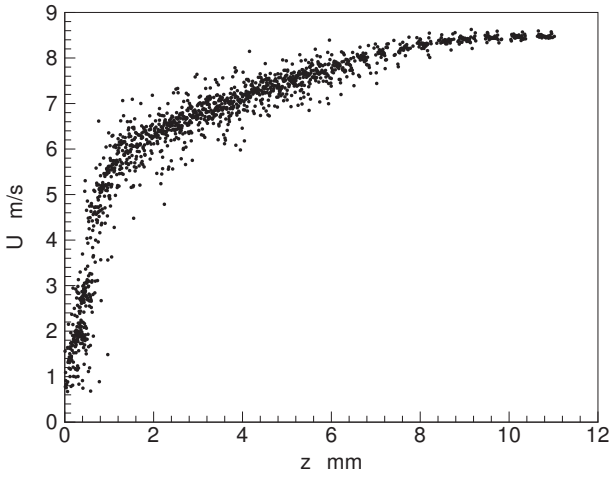

Figure 14: Averaged Velocity Profile in a Turbulent Boundary Layer

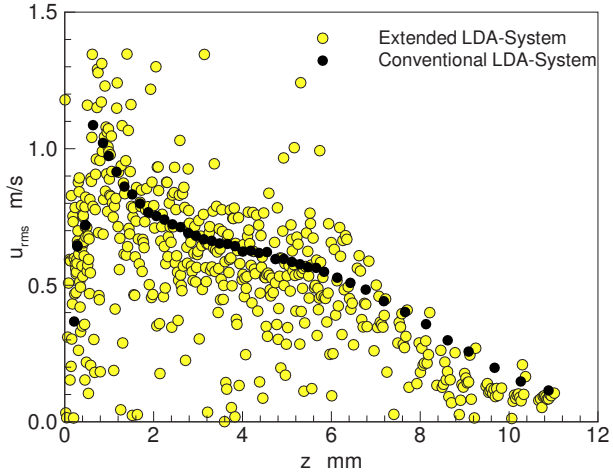

Figure 15: Distribution of Standard Deviation in a Turbulent Boundary Layer